PROCEEDINGS OF SPIE

SPIEDigitalLibrary.org/conference-proceedings-of-spie

Soft x-ray performance and fabrication of flight-like blazed transmission gratings for the x-ray spectrometer on arcus probe

Ralf Heilmann, Alexander Bruccoleri, Eric Gullikson, Randall Smith, Mark Schattenburg

Ralf K. Heilmann, Alexander R. Bruccoleri, Eric M. Gullikson, Randall K. Smith, Mark L. Schattenburg, "Soft x-ray performance and fabrication of flight-like blazed transmission gratings for the x-ray spectrometer on arcus probe," Proc. SPIE 12679, Optics for EUV, X-Ray, and Gamma-Ray Astronomy XI, 126790L (5 October 2023); doi: 10.1117/12.2676797

SPIE.

Event: SPIE Optical Engineering + Applications, 2023, San Diego, California, United States

Downloaded From: https://www.spiedigitallibrary.org/conference-proceedings-of-spie on 25 Oct 2023 Terms of Use: https://www.spiedigitallibrary.org/terms-of-use

Soft x-ray performance and fabrication of flight-like blazed transmission gratings for the X-Ray Spectrometer on Arcus Probe

Ralf K. Heilmann[a], Alexander R. Bruccoleri[b], Eric M. Gullikson[c], Randall K. Smith[d], and Mark L. Schattenburg[a]

[a]Space Nanotechnology Laboratory, MIT Kavli Institute for Astrophysics and Space Research, Massachusetts Institute of Technology, Cambridge, MA 02139, USA
[b]Izentis, LLC, Cambridge, MA 02139, USA
[c]Lawrence Berkeley National Laboratory, Berkeley, CA 94720, USA
[d]Center for Astrophysics, Harvard-Smithsonian Astrophysical Observatory, Cambridge, MA 02138, USA

ABSTRACT

In response to Astro2020 recommendations, NASA has issued an announcement of opportunity for an Astrophysics Probe Explorer. Arcus-Probe is a mission concept featuring two co-aligned high-resolution spectrometers, one for the soft x-ray band, and one for the far ultraviolet. This combination of instruments will provide unprecedented performance for the exploration of feedback that shapes the structure and influences the dynamics of our universe across many scales, ranging from galaxy clusters down to individual stars. In the soft x-ray band the X-Ray Spectrometer features four parallel channels, comprised of arrays of Silicon Pore Optics (SPO) and Critical-Angle Transmission (CAT) gratings. The channels will provide a combined effective area > 350 cm^2 near O VII (~ 470 cm^2 expected), and resolving power $R = \lambda/\Delta\lambda > 2500$ (~ 3500 expected) across the $\sim 12 - 50$ Å wavelength range. Light-weight, high-efficiency, blazed and alignment-insensitive CAT gratings have been shown to meet or exceed Arcus requirements for diffraction efficiency, open area, and effective resolving power. A total of $864 \sim 32 \times 32.5$ mm^2 CAT grating facets must be fabricated for Arcus, implying efficient volume production. We describe the x-ray testing and performance of the most recent flight-like grating facets, made from 200 mm silicon-on-insulator (SOI) wafers using tools compatible with volume production. Newly acquired SOI wafers with 100 nm device layer thickness control are expected to increase fabrication yields, and ongoing post-fabrication thinning of freestanding CAT grating bars promises increases in diffraction efficiency.

Keywords: Arcus, critical-angle transmission grating, x-ray spectroscopy, blazed transmission grating, soft x ray, grating spectrometer, high resolving power

1. INTRODUCTION

Imaging of celestial objects such as the planets of our solar system, stars, jets, nebulae, and galaxies inspire the popular imagination. However, most imaging detectors are incapable of measuring the energy of the incident photons accurately and precisely enough to draw clear-cut conclusions about the physical conditions and chemical abundances at the observed source. Clearly, high-resolution spectroscopy is compulsory if we want to understand the physics that control our universe. In agreement, the Astro2020 Decadal Review, "Pathways to Discovery in Astronomy and Astrophysics"[1] states: "Astronomy became astrophysics with the first spectrum. Spectroscopy determines compositions, magnetic field strength, space motion, rotation, multiplicity, planetary companions, surface structure, and other important physical traits...In the next decade, spectroscopy will be the dominant discovery tool for astronomy."

Further author information: (Send correspondence to R.K.H.)
E-mail: ralf at space.mit.edu, , URL: http://snl.mit.edu/

Optics for EUV, X-Ray, and Gamma-Ray Astronomy XI, edited by Stephen L. O'Dell, Jessica A. Gaskin, Giovanni Pareschi, Daniele Spiga, Proc. of SPIE Vol. 12679, 126790L · © 2023 SPIE · 0277-786X · doi: 10.1117/12.2676797

Downloaded From: https://www.spiedigitallibrary.org/conference-proceedings-of-spie on 25 Oct 2023
Terms of Use: https://www.spiedigitallibrary.org/terms-of-use

The soft x-ray band, covering the characteristic lines of the most abundant "metals" (O, C, Ne, Fe, N, Si, Mg, S), is especially fertile ground for studying the composition and dynamics of the warm and hot, highly ionized plasmas that trace crucial feedback processes across up to fifteen orders of magnitude in scale. Examples range from the accretion from protoplanetary disks onto young stars, through the mass flux and evolution of accretion-driven winds from the innermost regions around active galactic nuclei, to the formation and cycling of gas, metals and dust in and out of galaxies and clusters. More examples of astrophysical subjects best studied with high-resolution soft x-ray spectroscopy are described elsewhere.[2,3]

XRISM[4] is scheduled to be launched the day after this conference. It carries the Resolve imaging x-ray microcalorimeter with 36 30-arcsec pixels and energy resolution ΔE possibly as low as 5 eV at 6 keV. It is expected to provide very exciting high-resolution spectra for harder x rays, but $E/\Delta E$ drops off quickly at lower energies. By far the best technology for high-resolution spectroscopy in the soft x-ray band are grating spectrographs. However, the still-operating workhorse instruments aboard Chandra (High Energy Transmission Grating Spectrometer - HETGS)[5] and XMM-Newton (Reflection Grating Spectrometer - RGS)[6] are based on technology from a generation ago and have aged significantly over almost a quarter century in space.

The critical-angle transmission (CAT) gratings used for soft x-ray spectroscopy on Arcus are blazed transmission gratings. A CAT grating-based spectrometer combines the benefits of transmission gratings – low mass, volume and power (for thermal control), relaxed alignment and stability tolerances, reduced part count – with those of blazed reflection gratings (higher diffraction efficiency; use of higher diffraction orders, which boosts spectral resolving power). In addition, CAT gratings become highly transparent at higher energies and thus are able to pass useful x rays to a detector (CCD or microcalorimeter) at the telescope focus. The X-Ray Spectrometer (XRS) instrument on Arcus will furnish at least an order-of-magnitude improvement over HETGS and RGS, designed to provide an effective area > 350 cm^2 near O VII (~ 470 cm^2 expected), and resolving power $R = \lambda/\Delta\lambda > 2500$ (~ 3500 expected) across the $\sim 12 - 50$ Å wavelength range.[3,7] Small Arcus-like spectrometers with 12-m focal length silicon pore optics (SPO) and co-aligned CAT gratings have been demonstrated with $R > 10^4$ and diffraction efficiency in accordance with performance predictions for Arcus.[8,9]

The Chandra HETGS has 336 grating facets. The 200 nm-period phase-shifting High Energy Gratings (HEG) consist of gold bars with an aspect ratio (height/width) of about 4.25 on top of a polyimide membrane. The Arcus XRS calls for $864 \sim 32 \times 32.5$ mm^2 CAT grating facets (distributed over four parallel optical channels (OC) - see Fig. 1), where the 200 nm-period silicon CAT grating bars are freestanding with aspect ratios up to 100. Their challenging fabrication requires state-of-the-art tools from the MEMS (microelectromechanical systems) industry and capable tools from the semiconductor industry. For timely volume production, CAT gratings are deep reactive-ion etched (DRIE) from 200 mm diameter silicon-on-insulator (SOI) wafers with 4-6 μm thick device layers. Two key parameters that need to be controlled over the whole wafer are the etch angle (etch tool and recipe dependent) and the device layer thickness (SOI wafer dependent).

Figure 1. Left: Schematic of the Arcus XRS after deployment. X rays enter the forward assembly from the left into four parallel OCs through thermal precollimators, followed by SPO and CAT grating petals (not visible), propagate through the extendable boom, and are detected by CCD cameras mounted to the rear assembly (RA) on the right. The RA is mounted to the same deck as the UV spectrometer (not shown). Right: Perspective view of a SPO (top) and grating (bottom) petal pair. The grating petal is curved to follow a prescribed Rowland torus surface.

Downloaded From: https://www.spiedigitallibrary.org/conference-proceedings-of-spie on 25 Oct 2023
Terms of Use: https://www.spiedigitallibrary.org/terms-of-use

We present x-ray synchrotron diffraction efficiency data and etch angle results from two different 200 mm DRIE tools for ~ 6 μm deep CAT gratings with ± 1 μm thickness variation. Fabrication has begun on a new set of SOI wafers with ± 100 nm device layer thickness variation, which greatly reduces problems with under- or overetching in the crucial DRIE step. Some of these new gratings will feature thinner cross support bars, reducing x-ray losses.

Finally, we are experimenting with gentle post-fabrication thinning of freestanding CAT grating bars using repeated oxidation-vapor HF etch cycles. It is expected that x-ray testing of these thinned gratings will show increased diffraction efficiency.

2. CAT GRATING PRINCIPLE AND STRUCTURAL HIERARCHY

CAT gratings feature ultra-high aspect-ratio, freestanding grating bars with nm-smooth sidewalls.[10] The entire grating is inclined such that x rays of wavelength λ impinge on the grating bar sidewalls at graze angles θ below the critical angle for total external reflection θ_c (see Fig. 2). The diffraction angle β_m for the m^{th} diffraction order is given by the grating equation

$$\frac{m\lambda}{p} = \sin\theta - \sin\beta_m, \tag{1}$$

where p is the grating period. Diffraction orders near the direction of specular reflection from the sidewalls show increased efficiency (i.e., blazing). The small critical angles for soft x rays (typically on the order of 1-2 degrees) demand high-aspect ratio grating bars in order to intercept all incoming photons. Furthermore, we want the bars to be as thin as possible to minimize blockage and absorption. The grating period cannot be too large compared to the x-ray wavelength to obtain diffraction orders that can be sorted by order using the energy resolution of Si-based detectors. We initially chose a design with grating period $p = 200$ nm, grating bar depth $d = 4$ micrometers, and bar thickness $b \approx 60$ nm. Recently we demonstrated $d > 5.5$ μm.[11] Blazing is most efficient when $\tan\theta \approx (p - b)/d$. (For $d = 4$ μm this means $\theta \approx 2$ deg.)

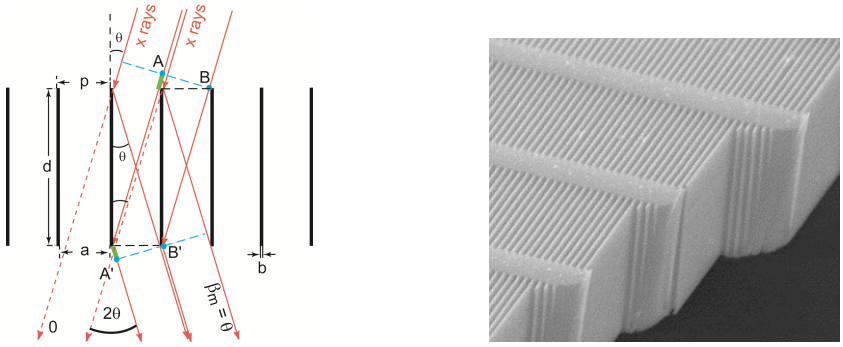

Figure 2. Left: Schematic cross-section through a CAT grating of period p. The m^{th} diffraction order occurs at an angle β_m where the path length difference between AA' and BB' is $m\lambda$. Shown is the case where β_m coincides with the direction of specular reflection from the grating bar sidewalls ($|\beta_m| = |\theta|$), i.e., blazing in the m^{th} order. Right: Scanning electron micrograph (SEM) of a cleaved CAT grating membrane showing top, cross-section and sidewall views of the 200 nm-period silicon grating bars and their monolithically integrated 5 μm-period L1 cross supports (x rays enter from the top and leave out the bottom).

CAT grating bars are not supported by a membrane, but freestanding. As seen on the right in Fig. 2, the bars are held in place by a monolithically integrated 5 μm-period Level 1 (L1) support mesh. Additional support structures are needed for the few-μm thin grating layer in order to manufacture large enough CAT gratings that can cover large areas on the order of thousands of square centimeters with a manageable number of gratings. Fig. 3 shows the additional, much thicker and stronger Level 2 (L2) hexagonal support structure on the scale of ~ 1 mm. The photograph on the right shows a so-called silicon grating membrane, etched from an silicon-on-insulator (SOI) wafer and featuring an additional 2 mm-wide Level 3 (L3) frame around the edge.

Downloaded From: https://www.spiedigitallibrary.org/conference-proceedings-of-spie on 25 Oct 2023
Terms of Use: https://www.spiedigitallibrary.org/terms-of-use

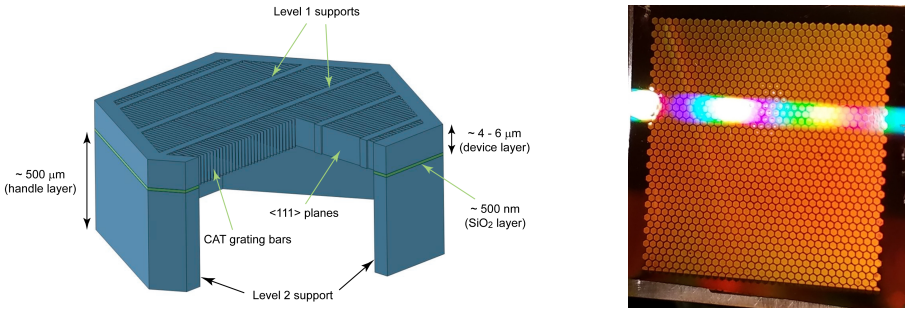

Figure 3. Left: Schematic showing the structural hierarchy of a CAT grating membrane (not to scale). Right: Photograph of an existing 32 x 32 mm^2 CAT grating membrane with back illumination to show the hexagonal L2 mesh, and with visible light diffraction due to the L1 mesh.

Each Si membrane is epoxy-bonded in four spots on the L3 frame to a flexured Ti frame, comprising a grating facet. The Ti frame is then mechanically fastened to a grating window, holding 4-6 aligned facets. For Arcus, each OC has a grating petal, which is populated by 40 grating windows. In the end all 216 grating membranes in the OC will be held tangentially to the same tilted Rowland torus within certain alignment tolerances.[7,12,13] Fig. 4 shows a 2×2 grating window with four Arcus-sized grating facets.

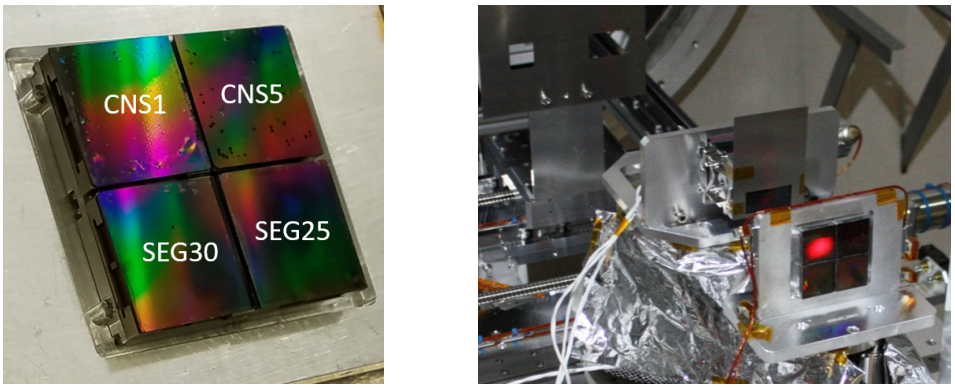

Figure 4. Left: Photograph of a 2×2 grating window, populated with four grating facets. Right: X-ray test setup at the MPE PANTER facility during laser alignment. Facet CNS1 is illuminated by the alignment laser coming through the SPO ca. 100 mm upstream from the grating window. See Heilmann et al.[9] for details.

3. CAT GRATING FABRICATION

CAT grating fabrication has been described extensively in previous work.[10,14–16] The key step that creates the ultra-high aspect-ratio grating bars is the DRIE of the patterned SOI device layer.

3.1 Grating Bar Tilt

The etch is the repeated iteration of the two-step Bosch process: a short etch with sulfur hexafluoride (SF_6) ions, followed by a short polymer deposition step that predominantly protects the sidewalls of the etched trench. The ions are accelerated toward the wafer, following the electric field lines between the plasma sheath and the biased wafer. If the field lines are not perpendicular to the wafer surface, the etch will proceed at an angle relative to the surface normal, resulting in grating bar sidewalls with a slight tilt, often called etch tilt, or in the case of gratings, bar tilt.

Since CAT gratings blaze at the angle of specular reflection from the grating bar sidewalls, bar tilt can lead to two main problems: First, if the bar tilt varies by more than a few tenth of a degree over the size of a grating,

Downloaded From: https://www.spiedigitallibrary.org/conference-proceedings-of-spie on 25 Oct 2023
Terms of Use: https://www.spiedigitallibrary.org/terms-of-use

then only part of the grating fulfills the optimum conditions for efficient blazing into desired diffraction orders, causing reduced diffraction efficiency. Second, if the magnitude of bar tilt is too large, the grating has to be rotated by a large angle for proper blazing, which can lead to large deviations of the grating surface from the ideal Rowland torus surface of the spectrometer, impacting spectral resolving power.[13]

In previous work we developed a small-angle x-ray scattering method in combination with laser reflection to measure bar tilt and found that our decades-old 100 mm etcher suffers from unacceptable bar tilt variations.[17] We have since etched 200 mm wafers with nominally 5.7 μm thick device layers on remote DRIE tools from two different manufacturers and measured bar tilt across the wafers. The etches were optimized for minimal mask erosion to reach the full depth of the device layer, and not for minimal bar tilt variations. As shown on the left in Fig. 5, both tools showed much more favorable and similar bar tilt variations in the central 80-120 mm, but better performance ($< \pm 0.2$ degrees over a whole 200 mm wafer) has been presented in the literature elsewhere.[18]

Ideally we would want to achieve no more than ± 0.2 deg of bar tilt across the central 150 mm of the wafer in order to easily put at least a 3×3 array of Arcus gratings in the center of a single wafer (see right of Fig. 5) without being impacted by excessive bar tilt. (Currently we assume that we can only use a 2×2 array from the center of each wafer.) Before going into production mode, etch recipes need to be optimized for a combination of minimal bar tilt, sufficiently small mask erosion, and straight (unbowed) grating bar profiles. A dedicated modern 200 mm DRIE tool would need to be available for this task, in combination with fast bar tilt metrology for quick recipe evaluation.

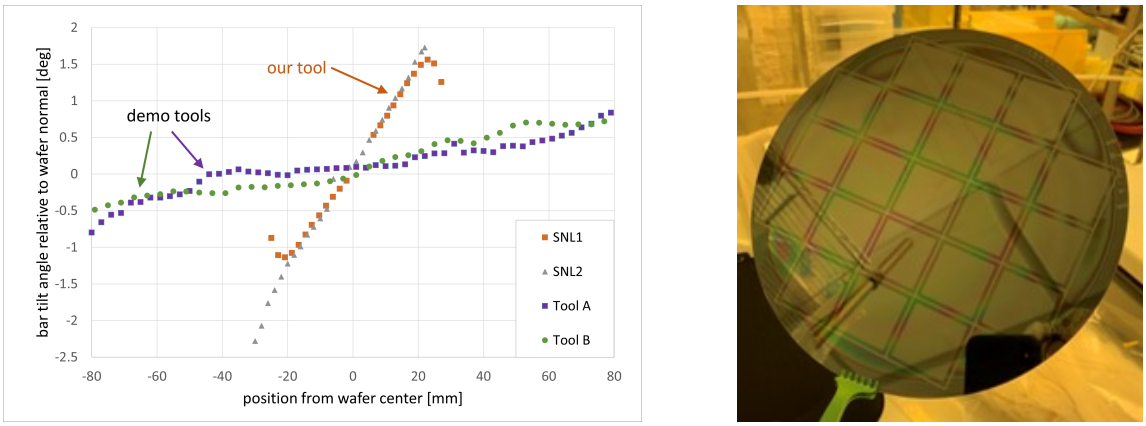

Figure 5. Left: Measured bar tilt for 200 nm-period CAT grating device layer DRIE across 100 and 200 mm wafers. "SNL1" and "SNL2" represent the performance of our DRIE tool, while "Tool A" and "Tool B" are results from etches performed by two different DRIE tool manufacturers. Right: Back side of 200 mm SOI wafer, patterned for 21 Arcus-sized CAT gatings.

3.2 Device Layer Thickness Variation

The SOI device layer thickness directly determines the height of the CAT grating bars. If this thickness varies significantly across the wafer it is difficult to achieve uniform etch results. In thicker areas the etch might not reach the buried oxide (BOX) layer, leading to leftover Si that can block soft x rays. In thin areas overetching can take place, which can lead to notching at the bottom of the device layer and destruction of the grating bars. Visible light transmission through a few microns of Si starts around 500 nm wavelength, blocking purple and most of the blue light, and giving the grating membrane a brownish to dark orange appearance when back-lit. Thickness variations between 5 and 7 micrometers change transmission on the order of 15% for a continuous Si film. We speculate that such large thickness variations are visible by eye in some of our gratings as variations in brightness (see Fig. 6).

Recently we acquired 200 mm SOI wafers with a quoted device layer thickness variation of ± 100 nm, a factor of ten better than our previous wafers. We are currently processing the first few of these wafers into freestanding gratings.

Downloaded From: https://www.spiedigitallibrary.org/conference-proceedings-of-spie on 25 Oct 2023
Terms of Use: https://www.spiedigitallibrary.org/terms-of-use

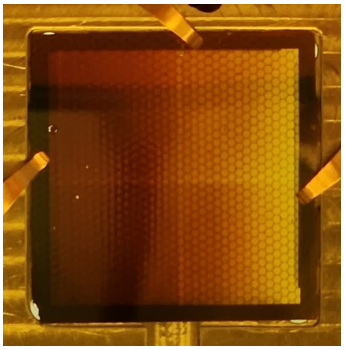

Figure 6. Grating sample SP5, back-illuminated by a diffuse white light source. Transmission increases from left to right, possibly due to a decrease in device layer thickness (nominally 6 μm thick). Underetching of the CAT grating bars on the left and overetching on the right as a result of varying device layer thickness could also contribute to the observed variation in light transmission. Also discernible are the boundaries between the four different exposure fields for this grating (marked by 10 μm wide Si lines in the OPL exposure), giving the appearance of faint cross hairs. (The darkest regions of the sample are due to reflection of objects in the lab behind the camera.)

3.3 Width of Level 1 Supports

The Level 1 (L1) supports form a 5 μm period cross support mesh. Our design L1 bar width for Arcus is 750 nm, which translates into 3 μm in the 4X optical projection lithography (OPL) mask. However, due to optical proximity effects during the OPL exposure step[16] the L1 bars ended up being 1.1 instead of 0.75 μm wide, leading to increased x-ray blockage. We designed a new mask with narrower L1 supports and now obtain an L1 bar width slightly below the desired value (see Fig. 7).

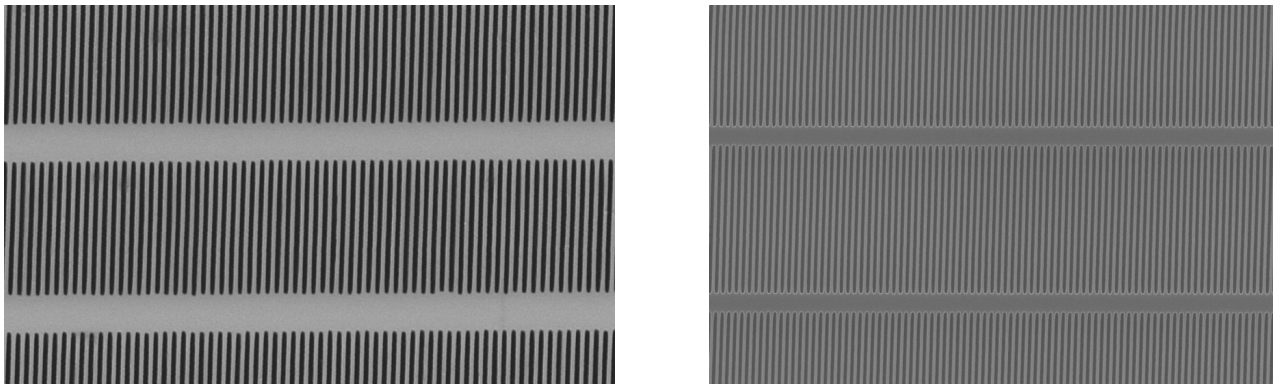

Figure 7. Top down scanning electron micrographs. Left: 200 nm-period CAT gratings etched into Si device layer (OPL performed with initial mask). L1 cross supports are about 1.1 μm wide. Right: 200 nm-period oxide pattern (pre-DRIE) obtained with new OPL mask. L1 cross supports are about 600 nm wide, increasing CAT grating area and x-ray throughput.

3.4 Manufacturing Readiness Level

Manufacturing Readiness Level (MRL) is used to assess the maturity of manufacturing readiness. In the years past we have systematically moved CAT grating fabrication from a manual "beakers and tweezer" approach - typical for university research labs - to a more industrial approach suitable for efficient volume production. A key step was the transfer of the initial grating and support structures patterning process from multiple manual interference lithography exposure steps on 100 mm wafers to the MIT Lincoln Laboratory (LL) Microelectronics Lab's 200 mm wafer fab, using 4X OPL. Many of our subsequent processing steps are also performed on 200 mm tools, but on campus at MIT.nano. Some of our steps are rather mature and compatible with MRL 6

Downloaded From: https://www.spiedigitallibrary.org/conference-proceedings-of-spie on 25 Oct 2023
Terms of Use: https://www.spiedigitallibrary.org/terms-of-use

("Capability to produce a prototype system or subsystem in a production relevant environment"). However, the key step that is lagging in MRL is device layer DRIE on 200 mm wafers, where we can only claim MRL 4 ("Capability to produce the technology in a laboratory environment"), due to lack of regular access to a modern 200 mm DRIE tool.

4. X-RAY PERFORMANCE

Here we summarize recent x-ray measurements at PANTER and discuss some new synchrotron data.

4.1 Flight-Like Grating Facets

We have recently produced several flight-like grating facets.[9] The grating membranes were made from 200 mm silicon-on-insulator (SOI) wafers, mostly using tools that are compatible with the volume production of CAT gratings.[16]

Four grating membranes were selected for bonding to frames. Bar tilt was measured for each membrane, and each membrane was individually rotated in yaw (the same angle as θ in Fig. 2) during bonding accordingly to achieve the same average bar tilt for each grating facet.[2] The resulting four facets were placed into a 2×2 grating window (see Fig. 4).

The window was partially illuminated through a focusing SPO in an Arcus-like setup at the MPE PANTER x-ray facility. All four gratings individually showed effective resolving power R_{eff} around 10^4. In addition, two of the gratings (SEG25 and SEG30) were illuminated simultaneously and demonstrated $R_{eff} > 10^4$ in the combined spectrum. This performance is superior to what is required for Arcus and makes us optimistic that R can reach 3500 for each full Arcus OC. Diffraction efficiency was also measured at PANTER and confirmed our modeling predictions, which are important inputs for Arcus effective area calculations. Details of these measurements have been presented previously elsewhere.[9]

4.2 Recent Synchrotron Data

Two years ago we presented x-ray data from the first CAT gratings that were close to 6 μm deep (samples SEG25 and SEG30, for example) and showed significantly higher diffraction efficiency than 4 μm-deep gratings.[11] Those gratings were deep-etched in the demo lab of a DRIE tool manufacturer and KOH polished at MIT. Recently a different DRIE tool manufacturer also provided us with deep etches of about 6 μm thick patterned device layers on 200 mm SOIs (sample SP5, as an example). Fig. 8 compares diffraction efficiency results between samples from both groups of etches. Due to small differences in bar tilt angles the measurements were not all performed at exactly the same sidewall incidence angles. Synchrotron measurements average over a small spot in the center of an L2 hexagon, and all of these samples had large device layer thickness uncertainties. Both sets of gratings show increased diffraction efficiency over the measured wavelength range compared to 4 μm-deep gratings. We find no striking difference between samples from the two groups of etches.

5. POST-FABRICATION GRATING BAR THINNING

A year ago we reported on initial experiments on gratings etched into bulk Si to investigate a gentle, vapor-based process to thin the grating bars that can be applied at the very end of fabrication. A native oxide layer automatically forms on silicon surfaces at room temperature in ambient air, where oxygen penetrates into the top few Si layers to form oxide, "consuming" some of the silicon. The width of the non-oxidized Si part of the grating bar is thereby reduced slightly. We remove the native silicon oxide using HF vapor, resulting in a slightly thinner bar. Over the course of a day or so a native oxide layer will reform, which we then remove again with HF vapor. After 30 cycles we observed thinning at a rate of ~1.4 nm/cycle on bulk Si samples. We are currently repeating these experiments with freestanding CAT gratings that have previously been tested at a synchrotron and will measure their diffraction efficiency again after 10-30 cycles or more, depending on the observed thinning.

Downloaded From: https://www.spiedigitallibrary.org/conference-proceedings-of-spie on 25 Oct 2023
Terms of Use: https://www.spiedigitallibrary.org/terms-of-use

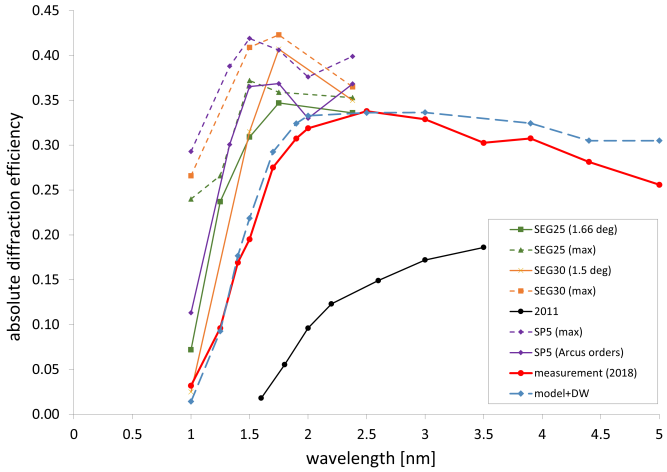

Figure 8. Absolute diffraction efficiency, including L1 blockage, as a function of wavelength. "max" sums up all the blazed diffraction orders, while the solid lines only include orders that would land on the Arcus XRS readout array. "2011" and "2018" show data from 4 μm-deep gratings taken in the respective years. "model + DW" refers to model predictions for 4 μm-deep gratings, including a Debye-Waller-type scattering factor.[16]

6. DISCUSSION AND OUTLOOK

The Arcus Probe concept is a powerful mission for trailblazing high-resolution spectroscopy in the soft x-ray and far UV bands, featuring mature technology. Here we described the status of CAT grating technology, which enables the XRS instrument.

Multiple flight-like CAT grating facets have been fabricated using methods and tools compatible with volume manufacturing. Resolving power demonstrated in Arcus-like configurations exceeds requirements, and diffraction efficiency meets model assumptions.[9]

Grating bar tilt - generated during DRIE - can restrict the SOI wafer area that is useful for CAT grating production. We can measure bar tilt and successfully correct for it during the facet bonding step,[9] as long as the tilt is not too large. We have shown that modern DRIE tools are capable of achieving low bar tilt across large fractions of 200 mm wafers, but we do not have regular or reliable access to such tools to refine our DRIE recipes.

Another yield-limiting factor - excessive SOI device layer thickness variations up to 25% - could be eliminated with better device layer thickness control. The first set of CAT gratings is currently being produced from 200 mm SOIs with $\pm$100 nm ($\sim$ 2%) thickness control.

We continue to explore ways to increase grating efficiency and throughput, leading to increased effective area for a given grating size. Reducing the area of L1 and L2 support structures is part of this work, and some of the latest gratings will have narrower L1 supports than the previous generation, which should lead to a relative increase in throughput of $\sim$ 12%. Deeper gratings have shown increased diffraction efficiency, especially at slightly smaller blaze angles than less deep gratings. This will mainly benefit CAT grating spectrographs for future potential missions such as Lynx.[19,20] Thinning of grating bars through repeated oxidation and HF vapor etch cycles also could increase effective area, both through reduced absorption by the grating bars and potentially reduced sidewall roughness. We are now applying this technique to freestanding gratings and expect to perform x-ray measurements on the resulting samples soon.

In summary, CAT grating technology and manufacturability have matured greatly over the last decade and a half. We are confident that CAT grating technology is ready to support a successful Arcus mission.

Downloaded From: https://www.spiedigitallibrary.org/conference-proceedings-of-spie on 25 Oct 2023
Terms of Use: https://www.spiedigitallibrary.org/terms-of-use

ACKNOWLEDGMENTS

We thank J. Gregory, D. Young, and R. Lambert (MIT Lincoln Lab) for helpful discussions. We gratefully acknowledge facility support from the Nanostructures Lab and MIT.nano. This work was supported by NASA grants 80NSSC19K0335, 80NSSC20K0780, and 80NSSC22K1904, and by the MIT Kavli Insititute for Astrophysics and Space Research. A part of this work used resources of the Advanced Light Source, which is a DOE Office of Science User Facility under contract no. DE-AC02-05CH11231. This work made use of the Shared Experimental Facilities at MIT supported in part by the MRSEC Program of the National Science Foundation under award number DMR 1419807.

REFERENCES

[1] National Academies of Sciences, Engineering, and Medicine, "Pathways to Discovery in Astronomy and Astrophysics for the 2020s," (2021).

[2] Heilmann, R. K., Bruccoleri, A. R., Burwitz, V., Cheimets, P., DeRoo, C., Garner, A., Gullikson, E. M., Günther, H. M., Hartner, G., Hertz, E., Langmeier, A., Mueller, T., Rukdee, S., Schmidt, T., Smith, R. K., and Schattenburg, M. L., "Flight-like critical-angle transmission grating x-ray performance for Arcus," in [*Space Telescopes and Instrumentation 2022: Ultraviolet to Gamma Ray*], den Herder, J.-W. A., Nikzad, S., and Nakazawa, K., eds., **12181**, 1218116, International Society for Optics and Photonics, SPIE (2022).

[3] Smith, R. K., "The Arcus Probe mission," in [*UV, X-Ray, and Gamma-Ray Space Instrumentation for Astronomy XXIII*], **12678**, International Society for Optics and Photonics, SPIE (2023).

[4] Tashiro, M., Maejima, H., Toda, K., Kelley, R., Reichenthal, L., Hartz, L., Petre, R., Williams, B., Guainazzi, M., Costantini, E., Fujimoto, R., Hayashida, K., Henegar-Leon, J., Holland, M., Ishisaki, Y., Kilbourne, C., Loewenstein, M., Matsushita, K., Mori, K., Okajima, T., Porter, F. S., Sneiderman, G., Takei, Y., Terada, Y., Tomida, H., Yamaguchi, H., Watanabe, S., Akamatsu, H., Arai, Y., Audard, M., Awaki, H., Babyk, I., Bamba, A., Bando, N., Behar, E., Bialas, T., Boissay-Malaquin, R., Brenneman, L., Brown, G., Canavan, E., Chiao, M., Comber, B., Corrales, L., Cumbee, R., de Vries, C., den Herder, J.-W., Dercksen, J., Diaz-Trigo, M., DiPirro, M., Done, C., Dotani, T., Ebisawa, K., Eckart, M., Eckert, D., Eguchi, S., Enoto, T., Ezoe, Y., Ferrigno, C., Fujita, Y., Fukazawa, Y., Furuzawa, A., Gallo, L., Gorter, N., Grim, M., Gu, L., Hagino, K., Hamaguchi, K., Hatsukade, I., Hawthorn, D., Hayashi, K., Hell, N., Hiraga, J., Hodges-Kluck, E., Horiuchi, T., Hornschemeier, A., Hoshino, A., Ichinohe, Y., Iga, S., Iizuka, R., Ishida, M., Ishihama, N., Ishikawa, K., Ishimura, K., Jaffe, T., Kaastra, J., Kallman, T., Kara, E., Katsuda, S., Kenyon, S., Kimball, M., Kitaguchi, T., Kitamoto, S., Kobayashi, S., Kobayashi, A., Kohmura, T., Kubota, A., Leutenegger, M., Li, M., Lockard, T., Maeda, Y., Markevitch, M., Martz, C., Matsumoto, H., Matsuzaki, K., McCammon, D., McLaughlin, B., McNamara, B., Miko, J., Miller, E., Miller, J., Minesugi, K., Mitani, S., Mitsuishi, I., Mizumoto, M., Mizuno, T., Mukai, K., Murakami, H., Mushotzky, R., Nakajima, H., Nakamura, H., Nakazawa, K., Natsukari, C., Nigo, K., Nishioka, Y., Nobukawa, K., Nobukawa, M., Noda, H., Odaka, H., Ogawa, M., Ohashi, T., Ohno, M., Ohta, M., Okamoto, A., Ota, N., Ozaki, M., Paltani, S., Plucinsky, P., Pottschmidt, K., Sampson, M., Sasaki, T., Sato, K., Sato, R., Sato, T., Sawada, M., Seta, H., Shibano, Y., Shida, M., Shidatsu, M., Shigeto, S., Shinozaki, K., Shirron, P., Simionescu, A., Smith, R., Someya, K., Soong, Y., Sugawara, K., Sugawara, Y., Szymkowiak, A., Takahashi, H., Takeshima, T., Tamagawa, T., Tamura, K., Tanaka, T., Tanimoto, A., Terashima, Y., Tsuboi, Y., Tsujimoto, M., Tsunemi, H., Tsuru, T., Uchida, H., Uchida, Y., Uchiyama, H., Ueda, Y., Uno, S., Vink, J., Watanabe, T., Witthoeft, M., Wolfs, R., Yamada, S., Yamaoka, K., Yamasaki, N., Yamauchi, M., Yamauchi, S., Yanagase, K., Yaqoob, T., Yasuda, S., Yoshida, T., Yoshioka, N., Zhuravleva, I., and Team, X. D., "Status of x-ray imaging and spectroscopy mission (XRISM)," in [*SPACE TELESCOPES AND INSTRUMENTATION 2020: ULTRAVIOLET TO GAMMA RAY*], DenHerder, J., Nikzad, S., and Nakazawa, K., eds., *Proceedings of SPIE* **11444**, SPIE (2021). Conference on Space Telescopes and Instrumentation - Ultraviolet to Gamma Ray / SPIE Astronomical Telescopes + Instrumentation Conference, DEC 14-18, 2020.

[5] Canizares, C., Davis, J., Dewey, D., Flanagan, K., Galton, E., Huenemoerder, D., Ishibashi, K., Markert, T., Marshall, H., McGuirk, M., Schattenburg, M., Schulz, N., Smith, H., and Wise, M., "The Chandra high-energy transmission grating: Design, fabrication, ground calibration, and 5 years in flight," *PUBLICATIONS OF THE ASTRONOMICAL SOCIETY OF THE PACIFIC* **117**, 1144–1171 (OCT 2005).

Downloaded From: https://www.spiedigitallibrary.org/conference-proceedings-of-spie on 25 Oct 2023
Terms of Use: https://www.spiedigitallibrary.org/terms-of-use

[6] den Herder, J., Brinkman, A., Kahn, S., Branduardi-Raymont, G., Thomsen, K., Aarts, H., Audard, M., Bixler, J., den Boggende, A., Cottam, J., Decker, T., Dubbeldam, L., Erd, C., Goulooze, H., Gudel, M., Guttridge, P., Hailey, C., Al Janabi, K., Kaastra, J., de Korte, P., van Leeuwen, B., Mauche, C., McCalden, A., Mewe, R., Naber, A., Paerels, F., Peterson, J., Rasmussen, A., Rees, K., Sakelliou, I., Sako, M., Spodek, J., Stern, M., Tamura, T., Tandy, J., de Vries, C., Welch, S., and Zehnder, A., "The reflection grating spectrometer on board XMM-Newton," *ASTRONOMY & ASTROPHYSICS* **365**, L7–L17 (JAN 2001).

[7] Günther, H. M., "Ray-tracing Arcus for performance and alignment tolerances," in [*UV, X-Ray, and Gamma-Ray Space Instrumentation for Astronomy XXIII*], **12678**, International Society for Optics and Photonics, SPIE (2023).

[8] Heilmann, R. K., Kolodziejczak, J., Bruccoleri, A. R., Gaskin, J. A., and Schattenburg, M. L., "Demonstration of resolving power $\lambda/\Delta\lambda > 10{,}000$ for a space-based x-ray transmission grating spectrometer," *APPLIED OPTICS* **58**, 1223–1238 (FEB 10 2019).

[9] Heilmann, R. K., Bruccoleri, A. R., Burwitz, V., deRoo, C., Garner, A., Günther, H. M., Gullikson, E. M., Hartner, G., Hertz, E., Langmeier, A., Müller, T., Rukdee, S., Schmidt, T., Smith, R. K., and Schattenburg, M. L., "X-ray performance of critical-angle transmission grating prototypes for the Arcus mission," *ASTROPHYSICAL JOURNAL* (2022).

[10] Bruccoleri, A., Guan, D., Mukherjee, P., Heilmann, R. K., Schattenburg, M. L., and Vargo, S., "Potassium hydroxide polishing of nanoscale deep reactive-ion etched ultrahigh aspect ratio gratings," *JOURNAL OF VACUUM SCIENCE & TECHNOLOGY B* **31** (NOV 2013).

[11] Heilmann, R. K., Bruccoleri, A. R., Song, J., Levenson, B., Smallshaw, B., Whalen, M., Garner, A., Heine, S. T., Marshall, H. L., Cook, M. T., Gregory, J. A., Lambert, R. D., Shapiro, D. A., Young, D. J., Gullikson, E. M., Nonaka, T., Uchida, A., Quijada, M. A., Hertz, E., Cheimets, P., Smith, R. K., and Schattenburg, M. L., "Manufacture and performance of blazed soft x-ray transmission gratings for Arcus and Lynx," in [*OPTICS FOR EUV, X-RAY, AND GAMMA-RAY ASTRONOMY X*], ODell, S., Gaskin, J., and Pareschi, G., eds., *Proceedings of SPIE* **11822**, SPIE (2021). Conference on Optics for EUV, X-Ray, and Gamma-Ray Astronomy X, San Diego, CA, AUG 01-05, 2021.

[12] Günther, H. M., Cheimets, P. N., Heilmann, R. K., Smith, R. K., and Collaboration, A., "Performance of a double tilted-rowland-spectrometer on Arcus," in [*UV, X-RAY, AND GAMMA-RAY SPACE INSTRUMENTATION FOR ASTRONOMY XX*], Siegmund, O., ed., *Proceedings of SPIE* **10397**, SPIE (2017). Conference on UV, X-Ray, and Gamma-Ray Space Instrumentation for Astronomy XX, San Diego, CA, AUG 06-08, 2017.

[13] Günther, H. M., DeRoo, C., Heilmann, R. K., Hertz, E., Smith, R. K., Wilms, J., and Collaboration, A., "Ray-tracing Arcus in Phase A," in [*SPACE TELESCOPES AND INSTRUMENTATION 2018: ULTRAVIOLET TO GAMMA RAY*], DenHerder, J., Nikzad, S., and Nakazawa, K., eds., *Proceedings of SPIE* **10699**, SPIE (2018). Conference on Space Telescopes and Instrumentation - Ultraviolet to Gamma Ray, Austin, TX, JUN 10-15, 2018.

[14] Bruccoleri, A. R., Guan, D., Heilmann, R. K., Vargo, S., DiPiazza, F., and Schattenburg, M. L., "Nanofabrication advances for high efficiency critical-angle transmission gratings," in [*OPTICS FOR EUV, X-RAY, AND GAMMA-RAY ASTRONOMY VI*], ODell, S. and Pareschi, G., eds., *Proceedings of SPIE* **8861**, SPIE (2013). Conference on Optics for EUV, X-Ray, and Gamma-Ray Astronomy VI as part of the SPIE Optics + Photonics International Symposium on Optical Engineering + Applications, San Diego, CA, AUG 26-29, 2013.

[15] Bruccoleri, A. R., Heilmann, R. K., and Schattenburg, M. L., "Fabrication process for 200 nm-pitch polished freestanding ultrahigh aspect ratio gratings," *JOURNAL OF VACUUM SCIENCE & TECHNOLOGY B* **34** (NOV-DEC 2016).

[16] Heilmann, R. K., Bruccoleri, A. R., Song, J., Cook, M. T., Gregory, J. A., Lambert, R. D., Shapiro, D. A., Young, D. J., Bradshaw, M., Burwitz, V., Hartner, G. D., Langmeier, A., Smith, R. K., and Schattenburg, M. L., "Toward volume manufacturing of high-performance soft x-ray critical-angle transmission gratings," in [*SPACE TELESCOPES AND INSTRUMENTATION 2020: ULTRAVIOLET TO GAMMA RAY*], DenHerder, J., Nikzad, S., and Nakazawa, K., eds., *Proceedings of SPIE* **11444**, SPIE (2021). Conference on Space Telescopes and Instrumentation - Ultraviolet to Gamma Ray / SPIE Astronomical Telescopes + Instrumentation Conference, DEC 14-18, 2020.

Downloaded From: https://www.spiedigitallibrary.org/conference-proceedings-of-spie on 25 Oct 2023
Terms of Use: https://www.spiedigitallibrary.org/terms-of-use

[17] Song, J., Heilmann, R. K., Bruccoleri, A. R., and Schattenburg, M. L., "Characterizing profile tilt of nanoscale deep-etched gratings via x-ray diffraction," *JOURNAL OF VACUUM SCIENCE & TECHNOLOGY B* **37** (NOV 2019).

[18] Barnett, R., Thomas, D., Song, Y., Tossell, D., Barrass, T., and Ansell, O., "A new plasma source for next generation mems deep si etching: Minimal tilt, improved profile uniformity and higher etch rates," in [*2010 Proceedings 60th Electronic Components and Technology Conference (ECTC)*], 1056–1059 (2010).

[19] Gaskin, J. A., Swartz, D. A., Vikhlinin, A., Ozel, F., Gelmis, K. E., Arenberg, J. W., Bandler, S. R., Bautz, M. W., Civitani, M. M., Dominguez, A., Eckart, M. E., Falcone, A. D., Figueroa-Feliciano, E., Freeman, M. D., Guenther, H. M., Havey, K. A., Heilmann, R. K., Kilaru, K., Kraft, R. P., McCarley, K. S., McEntaffer, R. L., Pareschi, G., Purcell, W., Reid, P. B., Schattenburg, M. L., Schwartz, D. A., Schwartz, E. D., Tananbaum, H. D., Tremblay, G. R., Zhang, W. W., and Zuhone, J. A., "Lynx x-ray observatory: an overview," *JOURNAL OF ASTRONOMICAL TELESCOPES INSTRUMENTS AND SYSTEMS* **5** (APR 2019).

[20] Güenther, H. M. and Heilmann, R. K., "Lynx soft x-ray critical-angle transmission grating spectrometer," *JOURNAL OF ASTRONOMICAL TELESCOPES INSTRUMENTS AND SYSTEMS* **5** (APR 2019).

Downloaded From: https://www.spiedigitallibrary.org/conference-proceedings-of-spie on 25 Oct 2023
Terms of Use: https://www.spiedigitallibrary.org/terms-of-use